C.E. Schwartz, T.G. Bryant, J.H. Cosgrove, G.B. Morse, and J.K. Noonan

A Radar for Unmanned Air Vehicles

Over the years airborne radars have proven their value as wide-area, nearly all-weather surveillance tools. Typically, airborne radars are large systems mounted in manned aircraft. Lincoln Laboratory, however, has built a very capable radar system that is compact and lightweight; the radar has been integrated into an unmanned air vehicle (UAV). The work is sponsored by the Army's Harry Diamond Laboratories and the Defense Advanced Research Projects Agency (DARPA). A significant component of the radar is a Lincoln Laboratory–designed programmable processor that performs moving-target detection on board the UAV. The onboard processing permits the use of a UAV data link that transmits kilobits per second of moving-target reports instead of tens of megabits per second of raw radar data. The system—the airborne portion of which weighs only 110 lb—detects and tracks moving vehicles such as tanks, trucks, and low-flying helicopters out to a range of 15 km, and classifies them at shorter ranges.

Unmanned air vehicles (UAV) have proven to be useful for observing activity on the ground without placing an air crew at risk. Using television cameras aboard small UAVs, the Israelis have successfully penetrated hostile air defenses and observed ground activity in enemy territories.

UAVs have several advantages over their manned counterparts. In addition to the obvious safety benefit, UAVs are relatively small and are thus difficult to detect either visually or with radars. Propeller-driven UAVs are also difficult to detect with an infrared (IR) sensor because their engines run at much cooler temperatures than jet engines. This combination of factors makes UAVs more survivable in a hostile environment than manned aircraft. The vehicles are also less expensive than their manned counterparts.

Current UAVs carry optical-sensor payloads—such as TV cameras and forward-looking infrared (FLIR) sensors—which are less susceptible to detection than active devices such as radars. Under favorable conditions, optical sensors can supply high-quality images of the ground for human interpretation. However, optical sensors suffer from a limited field of view and from severely reduced performance in adverse weather and battlefield smoke and dust conditions.

Radars, on the other hand, can be designed to rapidly scan large areas and they are less affected by weather, smoke, and dust. Without crossing international borders, long-range standoff surveillance radars, such as the Joint Surveillance and Target Attack Radar System (Joint STARS), can provide rapid surveillance of large areas of foreign territory. (Standoff radars are radars whose long range permits them to remain at a distance from the area under observation.)

In such militarily strategic regions as Central Europe and Korea, terrain and foliage masking can limit the view of standoff radars. Measurements taken in Central Europe (Fig. 1) [1] and masking studies in the Fulda region in West Germany [2] indicate that a radar with a depression angle of 11° can detect moving vehicles on roads radial to the sensor with about twice the probability of a radar with a depression angle of 3°. (A depression angle is the angle of the radar's line of sight below a horizontal plane.) Larger depression angles would result in even better visibility of the ground.

To avoid enemy air defenses, however, manned airborne systems must stay a con-

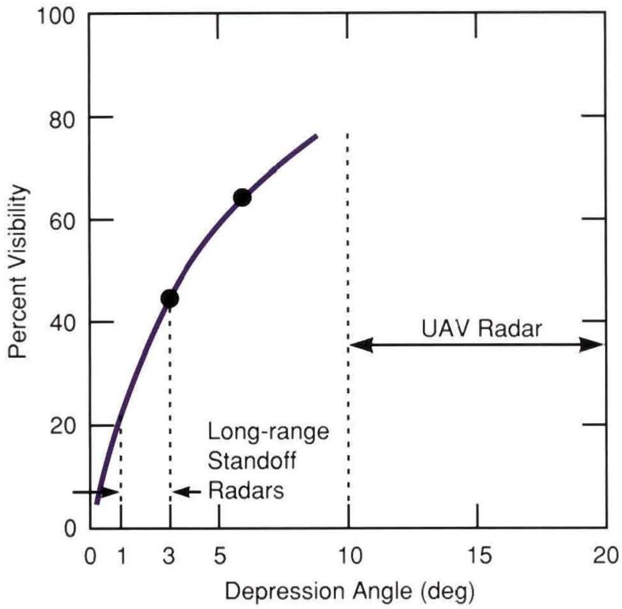

Fig. 1—Visibility of moving vehicles on radial roads versus radar depression angle. Radial roads are those roads which are radial (±20°) to the sensor. The depression angle is the angle of the radar's line of sight below a horizontal plane.

siderable distance behind the forward line of troops. This requirement makes it difficult for radars aboard manned aircraft to achieve large depression angles to the area of interest. Combining the attributes of a modern radar with the UAV's ability to penetrate hostile air space creates a valuable complement to Joint STARS. During a time of hostilities, Joint STARS could direct a UAV to explore critical areas blocked from view by terrain or foliage, or it could cue the UAV to provide a closer look at the activity in a particular area of interest.

If survivability becomes more of an issue, the survivability of UAVs could be increased with a number of countermeasures. For example, cheap radar decoys could be used to trick the enemy into firing expensive missiles at the decoys, or inexpensive escort UAVs could be used to attack enemy search radars.

In the earlier Netted Radar [3] and Advanced Airborne Radar [4] programs, Lincoln Laboratory demonstrated a network that provided accurate real-time display of battlefield activity. The network consisted of ground and airborne Moving Target Indicator (MTI) radars with modern programmable signal processors. The

Fig. 2—The Amber unmanned air vehicle (UAV), which is manufactured by Leading Systems, Inc.

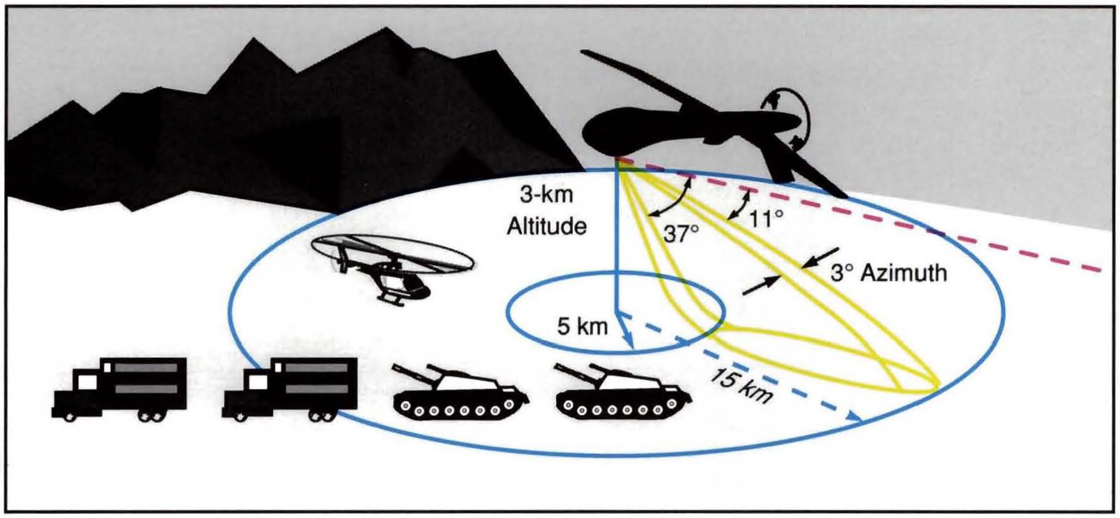

Fig. 3—UAV radar flight geometry. The UAV radar system has a 360° wide-area surveillance mode in which the radar antenna sweeps out an annular 5-km-to-15-km range swath every 18 s. At an operational altitude of 3 km, the swath corresponds to depression angles of 11° to 37°, thus affording excellent visibility of ground activity.

airborne radar system, however, was not practical for UAVs: the radar weighed 1200 lb and was connected via a wideband 10-Mb/s data link to a 40-ft ground van that contained a general-purpose minicomputer and a 1400-lb, 3-kW Westinghouse Programmable Signal Processor. The challenge of the current program was to perform the same functions as the earlier radar within the size, weight, power, and other constraints imposed by the UAV platform.

Lincoln Laboratory has built a compact MTI radar system configured as a payload for the Amber UAV (Fig. 2). (Amber was sponsored by the Defense Advanced Research Projects Agency [DARPA] and is manufactured by Leading Systems, Inc.) Although the radar is specifically designed for Amber it could be reconfigured to fit into other UAVs [5] that have the sufficient payload capacity.

The UAV radar system can detect and track moving tactical vehicles such as tanks, trucks, and low-flying helicopters out to a range of 15 km. The radar can also classify targets as tanks or trucks at shorter ranges when enough of the vehicle is visible. To reduce the data-link bandwidth from tens of megabits per second to less than ten kilobits per second, the system was designed with the signal processing performed on board by a high-speed programmable processor that currently operates at 108 million fixed-point operations per second (MOPS). Narrowband data links can be made more robust and jam-resistant than wideband data links. An onboard Inertial Navigation System (INS) accurately determines the UAV's position and attitude. This information plus the radar measurements on each of the detected vehicles permit the estimation of the locations of the detected vehicles.

The UAV radar system has a 360° wide-area surveillance mode in which the radar antenna sweeps out an annular 5-km-to-15-km range swath (Fig. 3) every 18 s. When the UAV radar is flying at an operational altitude of 3 km, the 5-km-to-15-km swath corresponds to depression angles of 11° to 37°, thus affording excellent visibility of ground activity. The UAV radar is designed to penetrate hostile airspace; the operational altitude of the radar puts it out of the range of the most common air defense systems such as antiaircraft guns and shoulder-fired IR missiles.

For initial tests and demonstrations, the UAV radar is being flown in a captive-flight mode in which the UAV fuselage is attached to and carried by a De Havilland Twin Otter airplane. All of the components needed to support free flight are in the UAV fuselage, but the Twin Otter

Table 1. UAV Radar Weight and Power Budget

	Weight	Power
Radar		
Transmitter	21	355
Receiver and exciter	10	95
Processor	55	400
Antenna system	14	75
Cables and connectors	10	25
	110 lb	**950 W**
Support Equipment		
Inertial Navigation System (including heat sink)	17	50
Data link	12	185
Altimeter and GPS receiver	9	20
Support structure	25	n/a
Cooling fans	2	150
	65 lb	**405 W**
Total	**175 lb**	**1355 W**

contains the instrumentation and display needed for system checkout.

An operator in a ground van controls the radar with commands via the data uplink. Moving-target reports are sent down the data link in real time for viewing on a display in the ground van. For instrumentation reasons, a wideband data link is being employed to communicate between the manned testbed and the ground van.

The radar is being flown and tested in an area west of Boston, and the moving vehicles on the roads are being used as test targets. Preliminary test results are encouraging: the locations of the

Table 2. UAV Radar Parameters

Radar type:	coherent-pulse Doppler
Frequency:	Ku-band
RF bandwidth (instantaneous):	10 MHz
Receiver noise figure:	7 dB
PRF (variable):	3 to 10 kHz
Range resolution:	15, 30, and 50 m
Linear dynamic range:	40 dB minimum
A/D quantization of I/Q video:	8 bits/channel
Antenna reflector type:	parabolic 18 in x 8 in
Rotary joints:	azimuth and elevation
Elevation pattern:	cosecant squared
Azimuth beamwidth:	3°
Scan speed (variable):	0°/s to 48°/s
Azimuth sidelobes:	–28 dB (maximum), –35 dB (average)
Peak gain:	30 dBi
Polarization:	horizontal

Table 3. Characteristics of the UAV Radar Basic Waveforms

1. Wide-area surveillance with moving-target detection
   - 360° scan every 18 s
   - 5-to-15-km range swath
   - 50-m-resolution waveform
   - 7-kHz maximum pulse repetition frequency (PRF)
2. Moving-target tracking
   - 30° scan every 5 s
   - 6-km range swath broken into two 3-km intervals
   - 15-m-resolution waveform
   - 4.4-kHz maximum PRF
3. Helicopter tracking
   - 25° scan every 2.5 s
   - 4-km range swath
   - 30-m-resolution waveform
   - 10-kHz maximum PRF

large numbers of detected targets correlate well with known roads.

General Description of the UAV Radar System

Capabilities, Specifications, and Features

The UAV radar is designed for the automatic detection and tracking of moving tactical ground vehicles as well as low-altitude, slow-flying aircraft such as helicopters out to a range of 15 km (Fig. 3). At that range, the Ku-band frequencies used have the capability to permit target detection in more than 90% of all weather conditions in Central Europe. Via a narrowband data link, the UAV radar can report moving targets to a ground van that is up to 30 km away. In an operational mode, the target data would be communicated via the UAV's standard data link, which might employ a radio relay to permit very long-range operation. The UAV platform can function either in a standoff mode, or in a penetrator mode over hostile airspace; the operating altitude of 3 km puts the UAV out of the range of inexpensive short-range air defense systems.

The total payload of the UAV radar requires less than 1400 W of prime power and weighs 175 lb (Table 1). The radar system alone weighs 110 lb; the remaining 65 lb are contributed by support equipment such as the INS, data link, and altimeter. In a free-flight configuration, the support equipment would normally be shared with the flight control system. The antenna subsystem, which weighs 14 lb and requires 75 W, is a mechanically rotating antenna with an 18-in-by-8-in dish, a 3° azimuth beamwidth, and a cosecant-squared-weighted elevation beam between −11° and −40°. Table 2 lists the UAV radar parameters.

The UAV radar has three basic linear FM pulse-compression (PC) waveforms and operates in a variety of modes to match different requirements for detection, tracking, and classification (Table 3). For the primary wide-area surveillance mode, the radar performs a 360° scan and detects moving targets in a 5-km-to-15-km range swath. A 50-m resolution waveform is used and the radar has a high probability of detecting targets in this mode.

In the moving-target tracking mode, the radar operates in a track-while-scan mode and a sector scan is chosen to focus on a specific geographic area of interest. The sector scan is centered on a specified coordinate in the Universal Transverse Mercator (UTM) coordinate

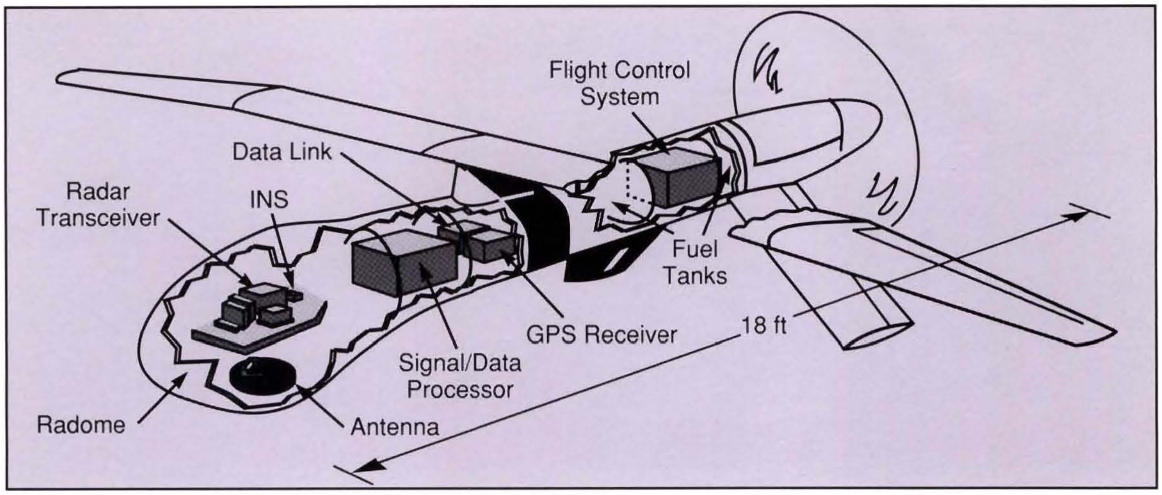

Fig. 4—Configuration of radar payload in Amber UAV.

system used by the U.S. Army. The 50-m resolution of the primary wide-area surveillance mode is not sufficient to resolve closely spaced targets. As a result, a higher resolution 15-m waveform is utilized in the moving-target tracking mode for better separation of individual vehicles.

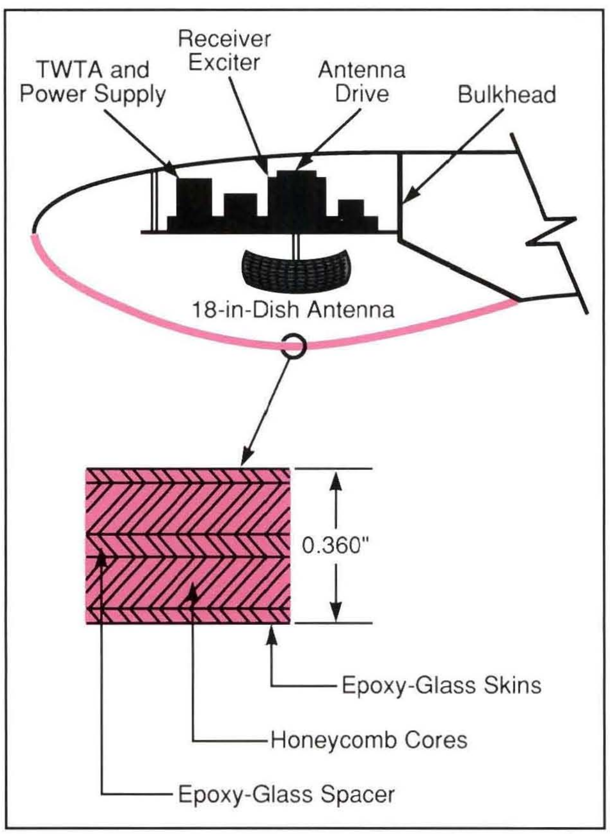

Fig. 5—Cross section of the low-drag, low-distortion UAV radome.

A high pulse-repetition frequency (PRF) was designed for the helicopter-detection mode to distinguish between helicopters and moving targets on the ground. The high PRF is intended for detecting individual flashes of the main rotor blade. A limited number of measurements on a Bell Jet Ranger helicopter showed that the main blade's flash could at times be detected. However, more data are required to quantify the helicopter-blade-detection performance that the UAV radar can achieve.

The Amber UAV Platform

Figure 4 shows the Lincoln Laboratory radar system that was configured to fly in the Amber UAV, which is 18 ft long and has a wingspan of 37 ft. The takeoff and landing gear of the Amber platform is retractable, which allows both an enlarged nose section for the radar payload and a radome below the payload. Working with Leading Systems, Inc., Lincoln Laboratory successfully addressed such system issues as weight distribution and balance, power requirements, cooling, and the implementation of a unique radome.

A major challenge was the construction of a radome that would satisfy various electrical, aerodynamical, mechanical, and fabrication requirements and constraints. It was critical that the UAV radome not significantly degrade the antenna pattern of the radar. But a conven-

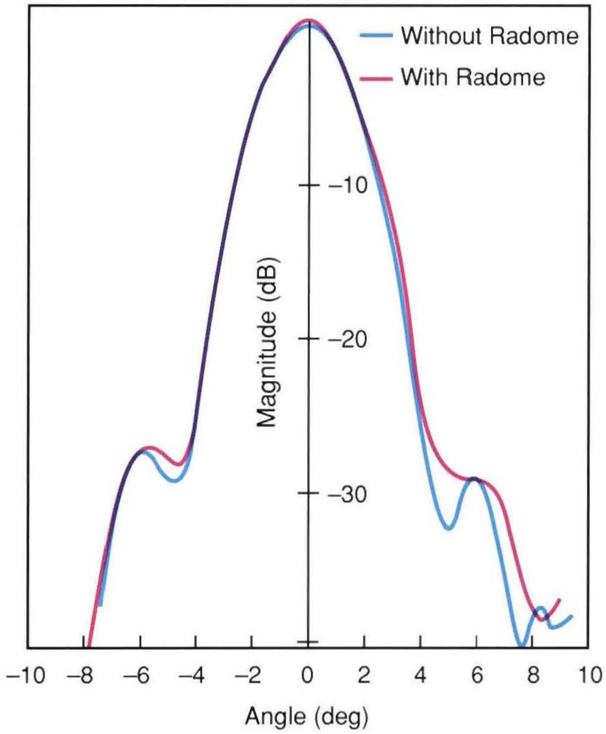

Fig. 6—Azimuth pattern of radar with and without radome.

tional spherical radome could not be used because such a structure would add a substantial amount of drag to the UAV platform and would thus significantly reduce the UAV's endurance. Lincoln Laboratory designed a low-drag radome in which the radar antenna pattern is maintained at incident angles that vary from a direction normal to the radome skin to a direction 75° off the normal. Figure 5 is a cross-sectional sketch of the design, which incorporates a multilayer sandwich configuration for the structure. Figures 6 and 7 show that the radome fabricated did not significantly alter the basic antenna patterns; note that the –28-dB azimuth sidelobe levels are unchanged when the radome is present.

System Components

Figure 8 is an overall block diagram of the basic components of the UAV radar system. The upper half of the figure shows the airborne components that are housed inside the UAV fuselage, including the processor, position-location equipment, and data link; the lower half of the figure shows the ground-based control equipment and the data-link tracker. The following sections describe the important components in detail.

Transceiver

The radar transceiver and antenna subassembly were built by the AIL division of Eaton Corp, and integrated with a traveling-wave-tube amplifier (TWTA) supplied by the Electron Technology Division of ITT. Lincoln Laboratory contributed to the design of a power supply and modulator that insures low spurious output. This requirement supports target-classification efforts that use low-level spectral signatures that can occur in the presence of strong clutter. As mentioned earlier, the transceiver has 50-, 30-, and 15-m-resolution waveforms to support the different MTI surveillance, tracking, and classification modes.

Figure 9 is a block diagram that highlights the major components of the Ku-band transceiver. Using one of the three pulse-compression (PC) networks, the system generates a linear FM transmit waveform in the exciter unit. The waveform is then upconverted to Ku-band,

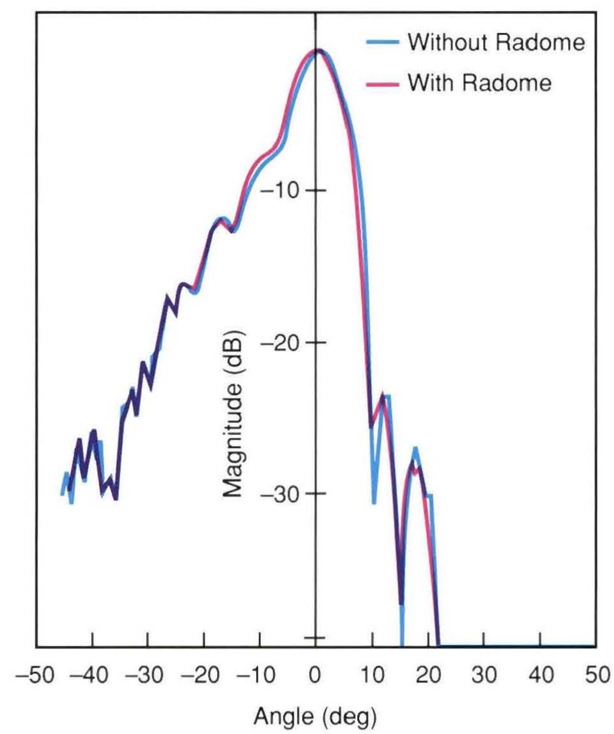

Fig. 7—Elevation pattern of radar with and without radome.

passed through the TWTA and duplexer, and sent out to the antenna. Phase stability is important for any Doppler radar; the single-sideband (SSB) phase noise characteristics of the UAV radar's L-band stable local oscillator (STALO) are –65 dBc/Hz at 100 Hz offset, –97 dBc/Hz at 1 kHz offset, and –130 dBc/Hz at 30 kHz offset.

The received signal comes into the duplexer/limiter and is downconverted, attenuated by the digitally controlled attenuator, and then passed to the appropriate PC network. Finally, the coherent detector produces in-phase and quadrature (I/Q) signals that are sent to the 8-bit flash A/D converters.

Figure 9 also shows other features of the transceiver implementation, including the frequency agility provided by the STALO, the voltage-controlled crystal oscillator for shifting the mean clutter frequency, the antenna-control interface, and the signal processor interface. To prevent receiver saturation while maintaining optimum A/D input signal levels, the transceiver has a digitally controlled IF attenuator in addition to the sensitivity time control (STC) provided by the duplexer/limiter. The limiter can provide attenuation from 0 to 50 dB.

Inertial Navigation System

The UAV radar system includes a small, commercial, lightweight INS. The UAV INS (Fig. 10), which is built by Litton, provides the platform-location and attitude information required for accurately locating detected targets in the UTM coordinate system. The INS is a strapdown version in that accelerometers and

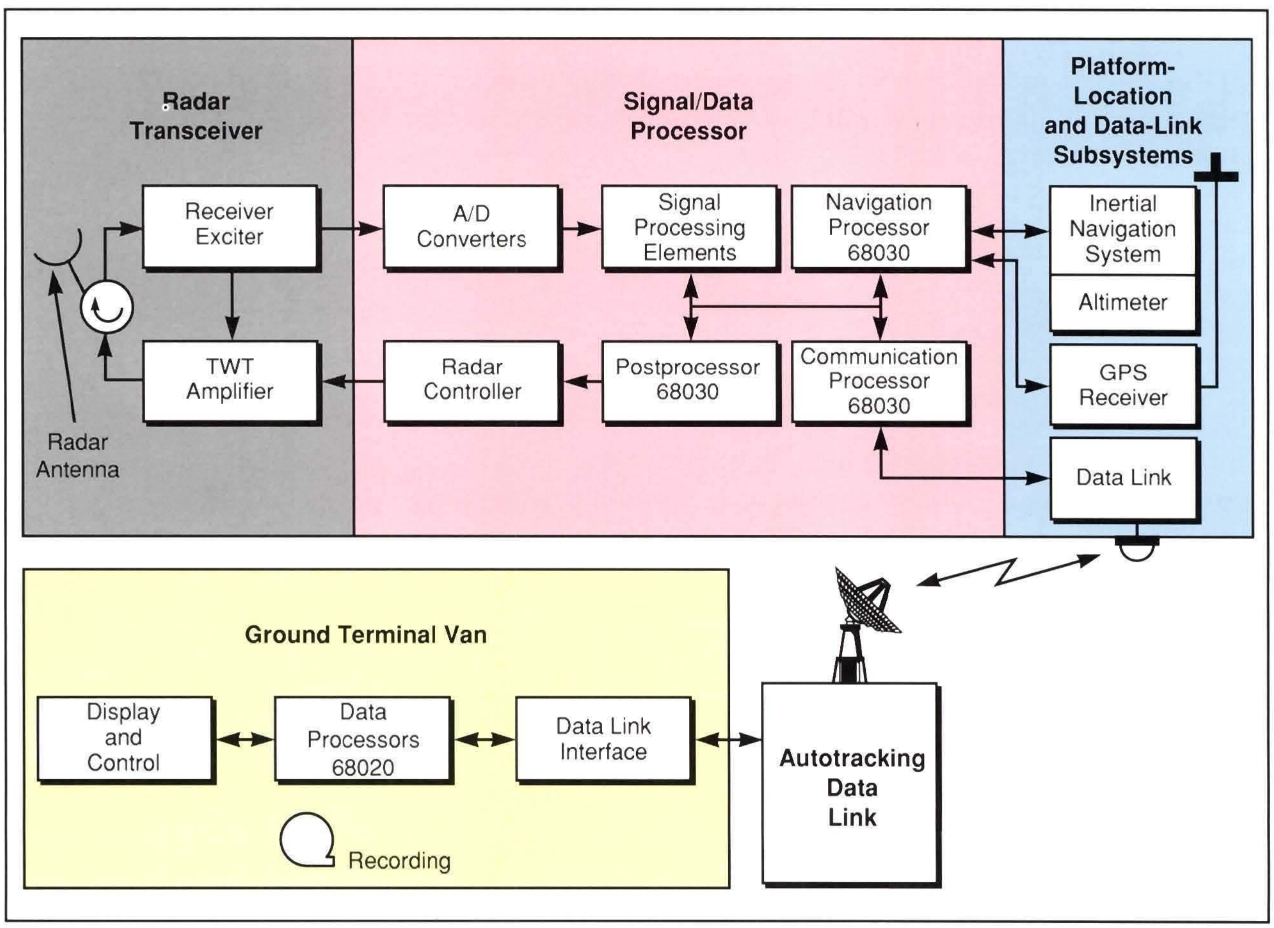

Fig. 8—Block diagram of UAV radar system. The upper half of the figure shows the airborne components that are housed inside the UAV fuselage, while the lower half shows the ground-based control equipment and the data-link tracker.

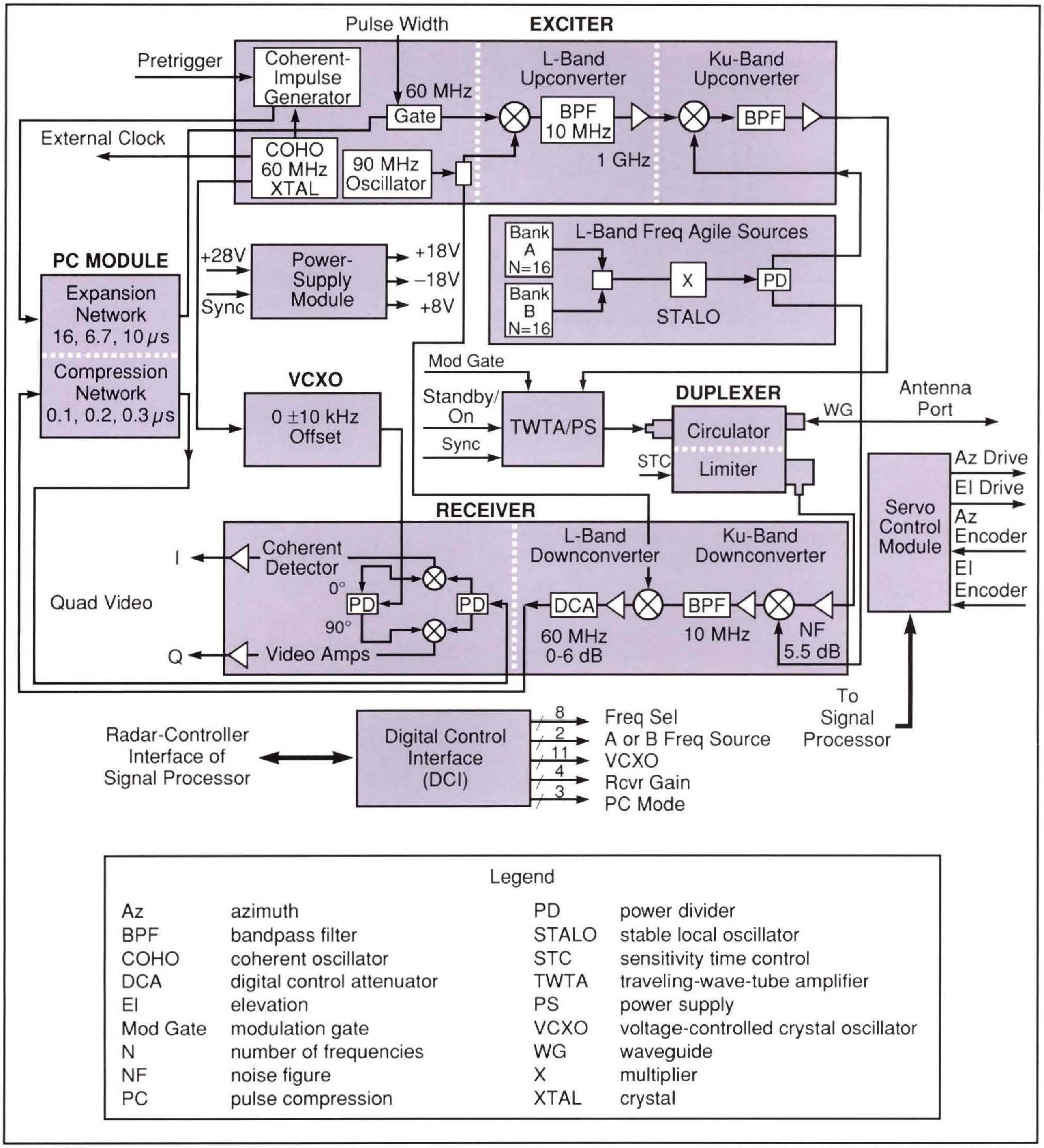

Fig. 9—Block diagram of UAV radar transceiver.

gyros are effectively strapped to the UAV's frame; i.e., the gyro-stabilized platform has been replaced by a gyro-stabilized direction-cosine computer program. Although the flight control system is separate from the radar payload, both would share the INS and data link in an operational configuration.

The INS accuracy is a function of the dynamics of the flight and the accuracy of position updates. Simulation of a typical flight indicates that the heading error will be approximately 0.15°, and the pitch and roll

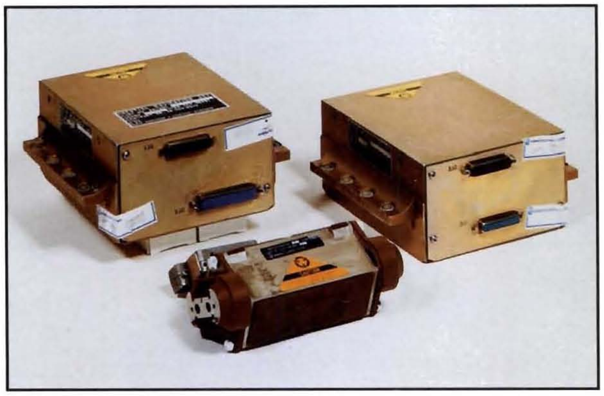

Fig. 10—Inertial Navigation System (INS): 7.5-in × 6.7-in × 3.2-in Inertial Measurement Unit (IMU) processor (upper left), 7.5-in × 6.7-in × 3.2-in navigation processor (upper right), and 6.3-in × 2.5-in × 3.1-in sensor assembly (bottom). The INS weighs 12.8 lb and requires 50 W of power. Cooling is by conduction and the system mean time between failure is 5200 h.

errors will both be 0.03°. If position updates are available and accurate to about 50 m, then the corresponding INS position error will be about 32 m.

Platform-Location Systems for INS Updating

Because the INS has inherent drift and precision errors, it must periodically be position corrected. We considered three methods for the calculation of accurate position estimates for INS updating. The methods used (1) range and bearing position estimates, (2) Global-Positioning System (GPS) receiver position estimates, and (3) multilateration position estimates.

Range and bearing position estimates. Most current systems estimate the location of a UAV in flight from the bearing information provided by the ground-based data-link tracking unit and a range measurement to the UAV. The accuracy of the technique, however, suffers from cross-range error, which increases as the range increases.

GPS-receiver position estimates. The best method of providing position updates to INS is with an onboard GPS receiver. This approach provides position information with a spherical error probability (SEP) of about 15 m, independent of the distance between the UAV and the ground-based terminal station. Greater accuracy could be achieved by placing a second GPS receiver at the ground station's known location. Differential operation could then provide an SEP of about 5 m by using the clear acquisition code. The new generation of integrated INS-GPS receiver packages that will soon be commercially available should make the GPS approach even more attractive. However, the GPS method is not currently feasible because existing GPS satellites only cover a certain geographic region for a few hours every day. About five GPS satellites were put into orbit from launches preceding the 1986 Challenger disaster. After a long hiatus during which no new GPS satellites were launched, five more were put into orbit in 1989, and the satellites are currently being launched at a rate of one every 80 days. Nonetheless, 21 GPS satellites are required for 24-hour coverage. After enough GPS satellites are available, we will evaluate a four-channel Motorola Eagle GPS receiver

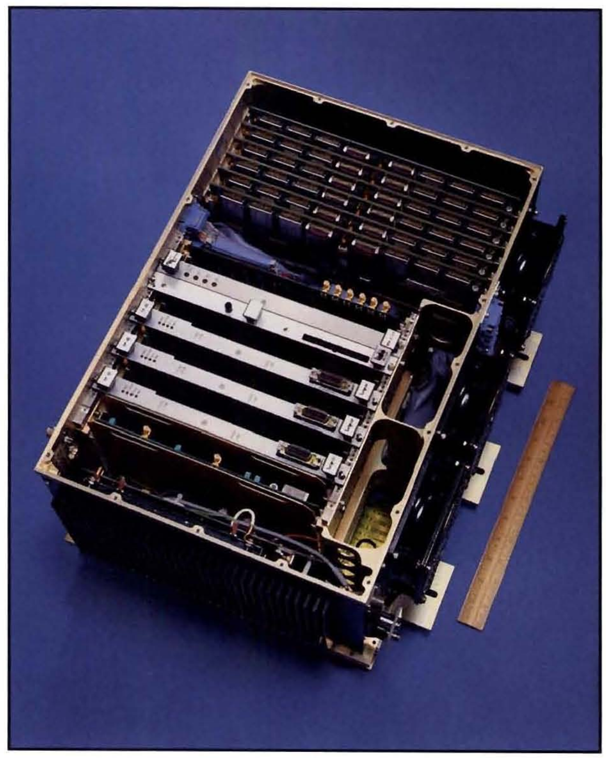

Fig. 11—Lincoln Laboratory's UAV-radar signal/data processor. The processor is programmable, weighs 55 lb, requires 400 W of power, occupies 1.6 ft^3, and currently performs 108 MOPS.

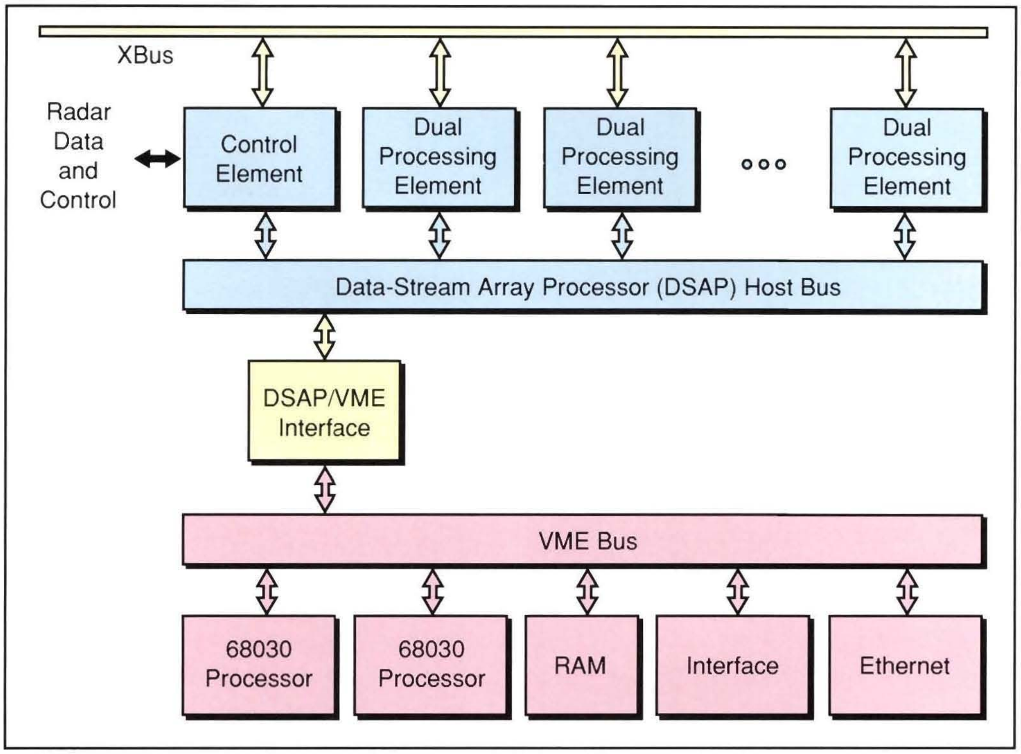

Fig. 12—Block diagram of the UAV radar programmable signal/data processor.

under typical UAV flight conditions.

Multilateration position estimates. Until more GPS satellites become available, we are emulating the accuracy of GPS position updates by using multilateration. With this technique, the platform carries a beacon interrogator that obtains range information from ground-based beacons placed at surveyed locations. The combination of beacon-based position estimates with INS filtering simulates the performance of the GPS receiver in that a 15-m SEP for the UAV location is provided.

UAV Signal/Data Processor

A major component of the radar development was a state-of-the-art, programmable, compact, high-speed signal/data processor [6] built by Lincoln Laboratory. The onboard processor (Fig. 11) converts tens of megabits per second of raw radar data into less than ten kilobits per second of moving-target reports. Because the processor is programmable, it can support a variety of modes and permits the easy addition of new algorithms. In the UAV radar system's general surveillance mode, the processor performs moving-target detection on a 10-km swath (250 40-m range cells) at a 6250 PRF (1,562,500 samples per second).

The processor weighs 55 lb, requires 400 W of power, and occupies 1.6 ft^3. The signal processing portion of the processor currently performs 108 MOPS. To achieve the small size and low power consumption, two custom VLSI chips were used and all of the arbitration logic between the custom chips and data memory were implemented on a custom gate array.

The processor is a complete system in the sense that it provides not only for signal processing, but also for the acquisition of radar data and the generation of radar control and timing signals. In a single chassis, the processor incorporates the radar's analog-to-digital (A/D) converters and interfaces to the data link, INS, and altimeter.

Processor Hardware

Figure 12 is a general block diagram that shows each type of board in the processor.

Custom dual-processing-element (PE) boards that are 12 in × 6 in perform the high-speed signal processing. If more signal processing capability is needed, the architecture allows additional dual-PE boards. The custom control-element (CE) board distributes raw radar samples to the PEs via a high-speed parallel bus capable of operating at 10 million 32-bit words per second. The CE board, which uses one of its programmable custom chips as the radar controller, also serves as the interface between the PEs and two commercial VME single-board computers built by the Tadpole Co. The Tadpole boards, which use Motorola 68030 microprocessors, provide general-purpose processing capability for a number of tasks: postdetection processing (described in the following section), data communication, navigation functions, and control of the radar's mode of operation. When the UAV is in captive-flight operation, a chip on the Tadpole board supports the Ethernet interface to the manned aircraft. The chip also provides a diagnostic interface that can be used when the UAV is on the ground and in free-flight configuration. A commercial 4-MB RAM board with a battery backup stores the real-time application and diagnostic software that is needed.

The chassis for the UAV processor (Fig. 11) contains six dual-PE boards. Each of the 12 PEs can be independently programmed to perform different functions concurrently. In our application we have chosen to partition the problem so that each PE is performing the same moving-target detection or other algorithm on a different portion of the range swath. If a PE fails it can be turned off and a reduction in the range swath being processed would result.

It is interesting to note that only about one-third of the processor chassis (and less than 100 W of power) is devoted to the custom programmable signal processing and the remaining two-thirds to the VME backplane. It should also be noted that many of the VME slots are not needed. Thus, with no increase in chassis size, we could double the signal processing capability of the processor by doubling the number of PE boards.

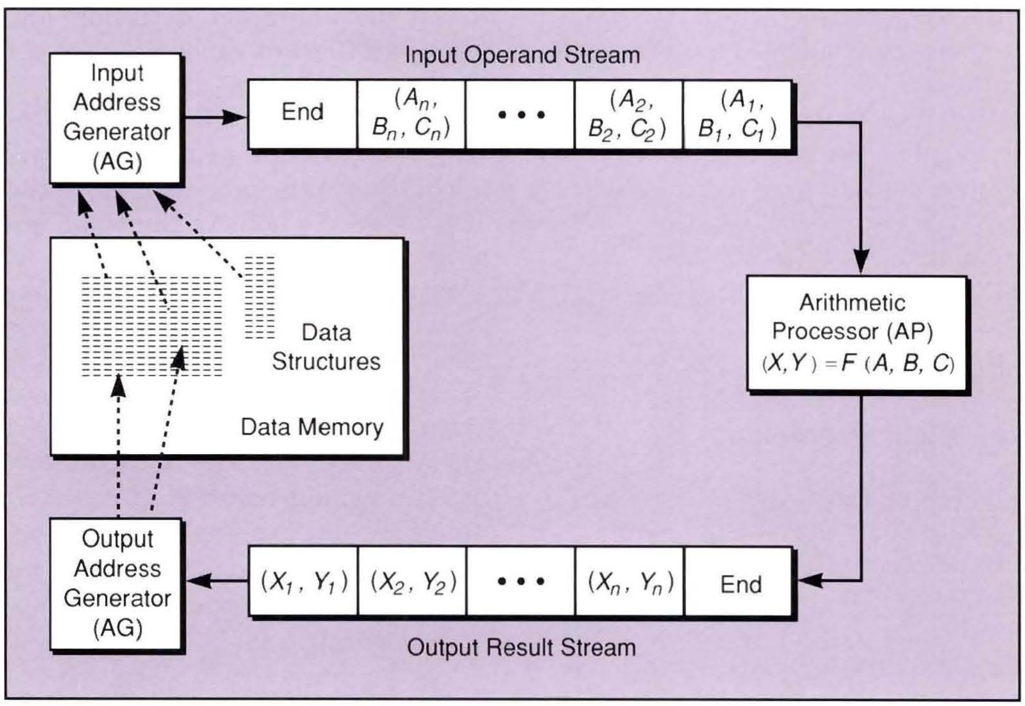

Fig. 13—Processing-element (PE) vector flow of data between the data memory and the arithmetic processor (AP).

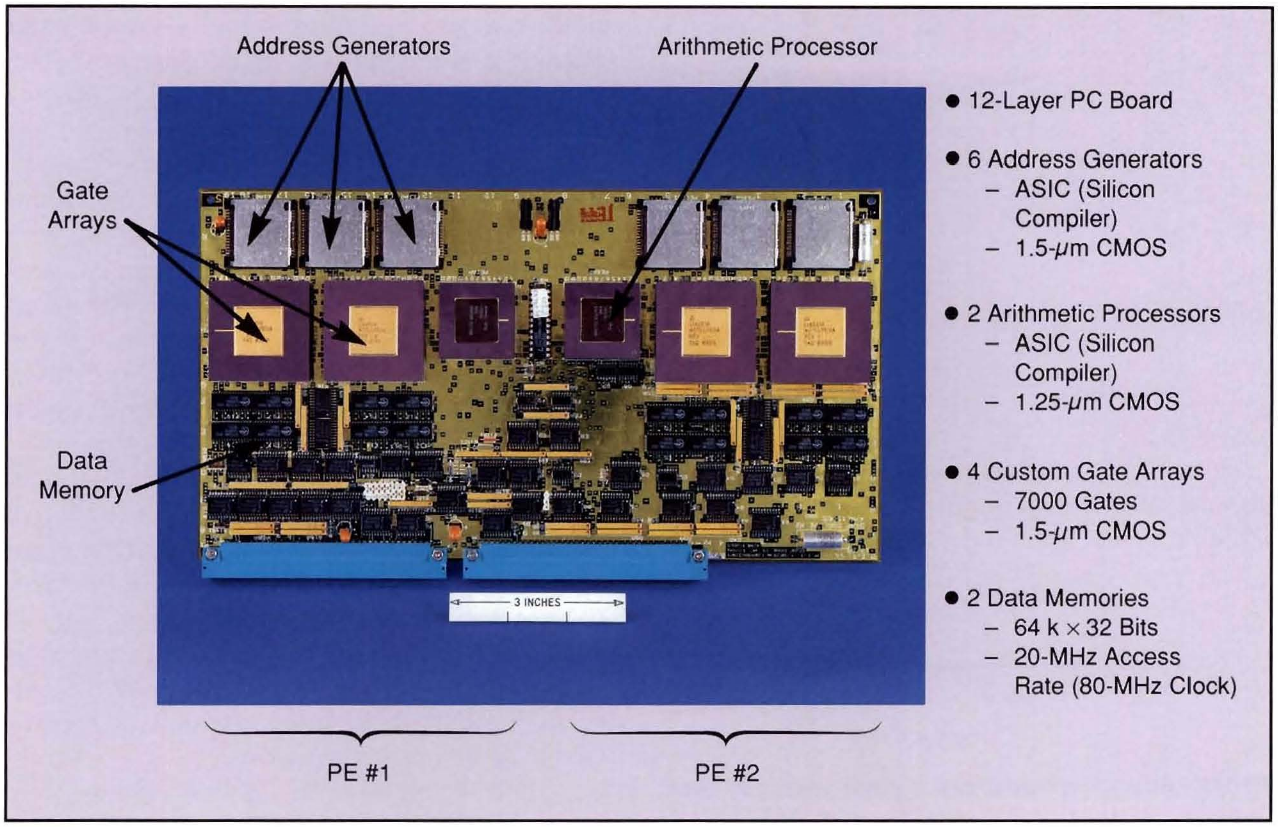

Fig. 14—The dual-processing-element (PE) board. The board operates at 60 MOPS (80-MHz clock speed), requires less than 10 W, and weighs 24 oz. The speeds and power specifications assume the latest versions of the AG chip (which has already been incorporated onto the board) and AP chip (which has been designed and is currently being fabricated).

The PE boards contain two types of programmable custom VLSI chips: an arithmetic processor (AP) and an address generator (AG). Both chips have on-chip instruction memory. Figure 13 depicts the flow of data between the PE's 64k × 32-bit data memory and the AP. The AP performs algorithmic calculations without regard for the addresses in the data memory of the inputs or the outputs. From the data memory, an input AG chip fetches the input stream of operands for the AP and a separate output AG chip stores the output stream of results back into the memory. A third AG chip selects raw radar samples for the appropriate ranges from the high-speed bus and places the samples in the memory for subsequent MTI processing. There are FIFO buffers on the input and output sides of the APs so that an AG need only match the average data rate of the AP to keep the AP running at full efficiency. The separation of the address and arithmetic calculations into asynchronous processes via the FIFOs greatly facilitates the optimization of complex signal processing algorithms. This feature is a significant advance of this signal processor architecture.

Lincoln Laboratory designed the AG and AP chips and originally implemented them in 3-μm NMOS technology. The chips are currently being reimplemented in smaller-geometry CMOS technology. Figure 14 shows the latest version of the PE board.

Processor Software

The signal processor's real-time application software uses Doppler filtering to detect moving targets. To remove DC biases and gain imbalances from the I/Q radar channels, the signal processing program generates a table that calibrates the incoming I/Q 8-bit A/D samples in real-time via a table lookup. In the calibration

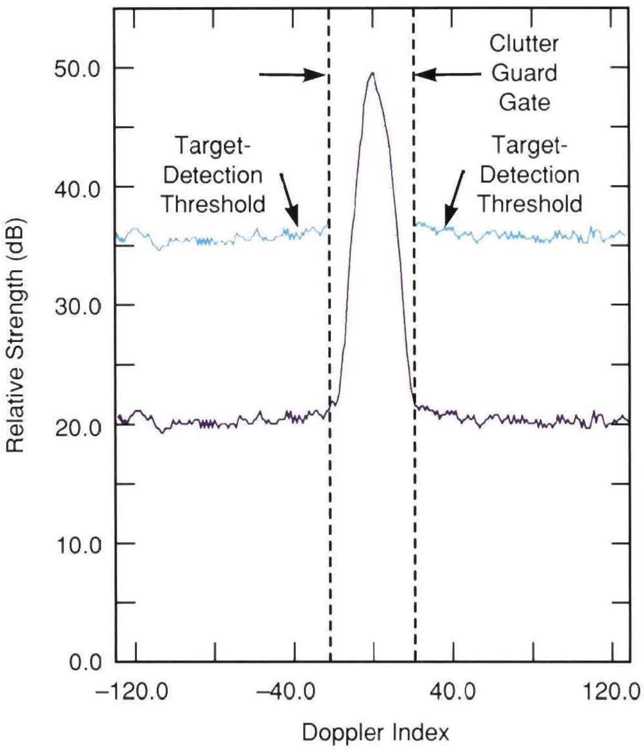

Fig. 15—Strength of radar return signal averaged over range versus Doppler-filter number. A target-detection threshold 15 dB above the average noise level and a four-filter guard band around the clutter have been added. Ignoring the filters within the guard band in the detection process insures that clutter is not detected.

process, which is performed on board the UAV while the vehicle is in flight, 30,000 samples of radar ground-clutter data are used to determine the DC biases, gain imbalances, and orthogonality of the I/Q radar channels. The calibration process assumes that (1) the amplitudes in each channel should add up to zero if there is no DC bias, (2) a difference in power indicates a difference in gain between the channels, and (3) the I/Q samples should be uncorrelated if the channels are orthogonal.

The program then checks for A/D saturation, performs a Hamming-weighted 64- or 256-point FFT, estimates the noise level on a filter-by-filter basis, and determines the position and width of clutter in Doppler space. Each Doppler filter is averaged over range to derive a noise estimate for the setting of detection thresholds and to determine the location and width of clutter. The signal processing program detects targets by setting thresholds relative to the average noise level in those filters which do not contain clutter. Detections are then reported to the postprocessor.

Figure 15 is a plot of the filters averaged over range in which the x-axis is the 256 Doppler filters. A target-detection threshold 15 dB above the average noise level has been plotted. From this averaged spectrum, those Doppler filters which contain clutter (in Fig. 15, the filters represented by the Doppler indexes ranging from –20.0 to 20.0) are determined. Such filters are ignored in the detection process to insure that clutter is not detected.

Figure 16 is a blowup of the bell-shaped ground clutter curve of Fig. 15 with the x-axis converted to meters per second. The figure shows the substantial width of clutter velocity that occurs at broadside. In contrast, Fig. 17 shows the clutter spectrum when the angle between the radar beam and the UAV velocity vector is small—a direction in which the spectral width of clutter is narrowest.

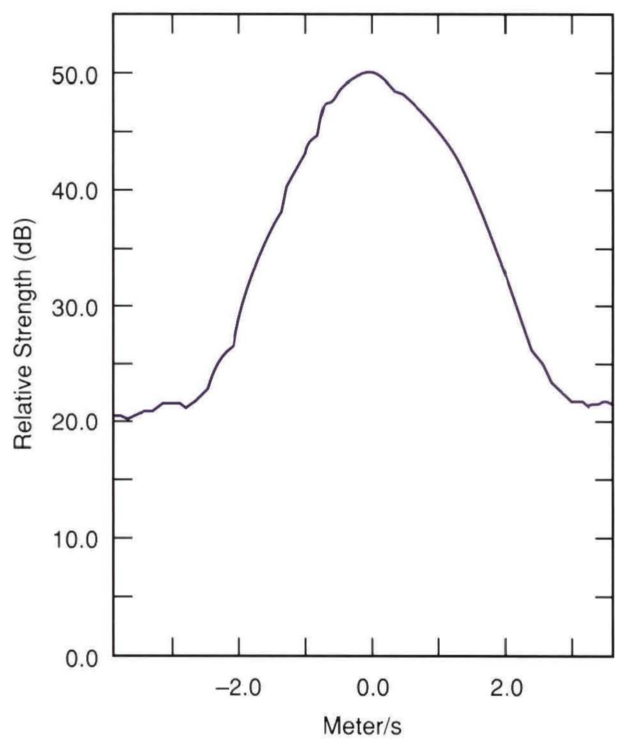

Fig. 16—Blowup of the bell-shaped clutter curve of Fig. 15. Note that the x-axis has been converted to meters per second. The substantial clutter precludes the detection of targets whose component of velocity along the radar's line of sight falls in the clutter spectrum.

The spectral width of clutter results from the varying clutter velocities that are contained within the radar's 3° azimuth beamwidth, i.e., the component of the platform velocity vector at different angles within the beam. This spectral width of clutter varies significantly as the angle between the radar beam and the UAV velocity vector changes because of the 360° rotation of the radar antenna. Adaptive estimation of the clutter width, as implemented in the processor, provides good clutter suppression while allowing for low-speed target detection at the more favorable angles. Figure 18 shows the expected sinusoidal variation of the clutter-masked ground speeds as a function of the radar azimuth angle. The nose of the plane is at 0°; thus 90° and 270° represent the radar's looking at clutter broadside to the aircraft. In the figure, the curve and the shaded region below the curve represent ground speeds that are masked by clutter and are ignored in the target-detection process. For example, if the radar is at an azimuth of 300°, objects traveling at a ground speed of less than about 1.5 m/s will be masked by clutter. Note that at an azimuth of 200° the nose wheel of the Twin Otter blocks the radar and thus removes the data used to derive clutter width.

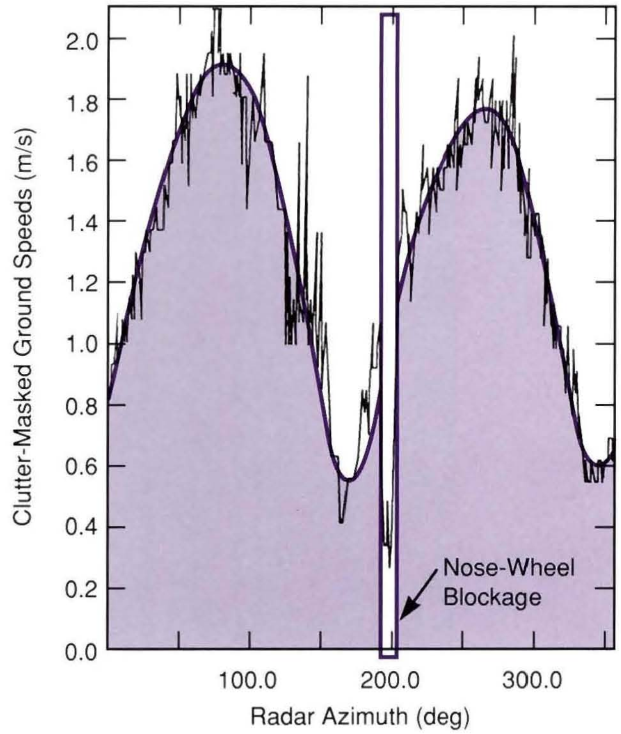

Fig. 18—Clutter-masked ground speeds as a function of the radar azimuth angle. The nose of the plane is at 0°; thus 90° and 270° represent the radar's looking at clutter broadside to the aircraft. In the figure, the curve and the shaded region under the curve represent ground speeds masked by clutter. For example, if the radar is at an azimuth of 300°, objects traveling at a ground speed of less than about 1.5 m/s will be masked by clutter. The figure was obtained at a UAV-platform ground speed of about 81 knots.

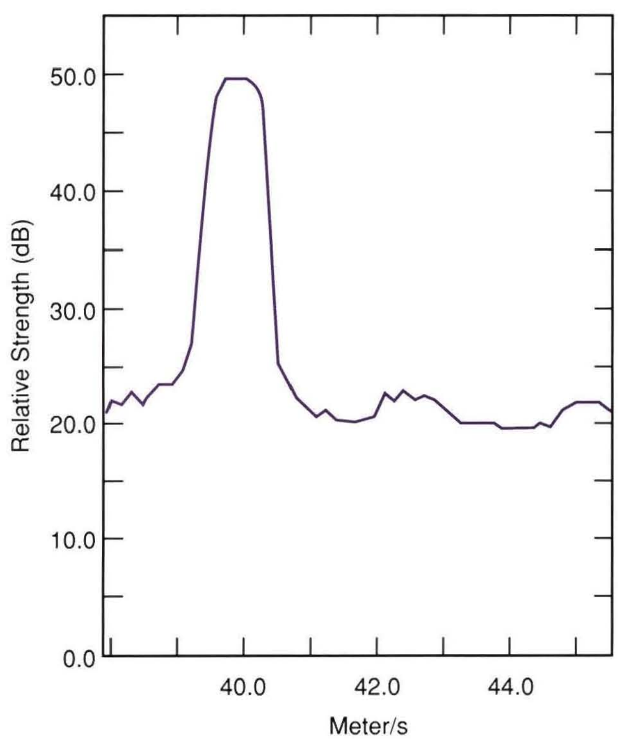

Fig. 17—Averaged clutter strength versus Doppler velocity for the case in which the radar antenna is pointing along the UAV platform's velocity vector. Note that the velocity width of clutter in this figure is much narrower than that of Fig. 16.

The velocity extent of clutter at broadside would have been narrower if the UAV platform had traveled at a slower speed. The results of Fig. 18 were obtained with the Twin Otter flying at a ground speed of 81 kn. (Note: We tried to simulate free-flight operating conditions as much as possible. However, because of physical limitations the Twin Otter could not be flown as slowly as the operating speed of the UAV.) Thus, because the operating speed of the UAV is 60 to 70 knots (kn), the performance of the UAV radar in free-flight operation will be better than that indicated by Fig. 18 in that the ampli-

Fig. 19—De Havilland Twin Otter aircraft carrying UAV fuselage.

tude of the curve will be reduced by the ratio of the UAV speed to the Twin Otter speed.

More computationally intensive algorithms could be implemented to detect low-speed targets that fall within the clutter spectrum. The algorithms would have to separate the slow-moving targets from natural clutter such as wind-blown trees and large man-made structures such as buildings and water towers.

During postprocessing, the moving-target detections are grouped into centroids based on their proximity in range, azimuth, and Doppler velocity. The position of each moving target with respect to the radar is determined by an average of the ranges and azimuths of the detections weighted by the logarithms of their amplitudes. The postprocessing program uses platform heading and position information from the INS along with range and azimuth estimates to determine the UTM position of each moving-target centroid. This general-purpose postprocessing is performed on two Motorola-68030-based single-board computers.

In addition to real-time application software, we have developed a significant amount of support software, including

- a software simulation of the hardware (the simulation permitted the development of application software and the alteration of the hardware design *prior* to the availability of the hardware),
- an assembler to support the development of application software in a symbolic language,
- a software and hardware debugger and a package of hardware diagnostic programs, and
- a real-time UNIX-like operating system to support multitasking on the multiple commercial single-board computers.

UAV Captive-Flight Testing

For captive-flight testing of the radar payload, an Amber UAV fuselage was attached to a De Havilland Twin Otter aircraft (Fig. 19). Although initial tests have been partially supported by instrumentation aboard the Twin Otter aircraft, the aircraft will ultimately provide

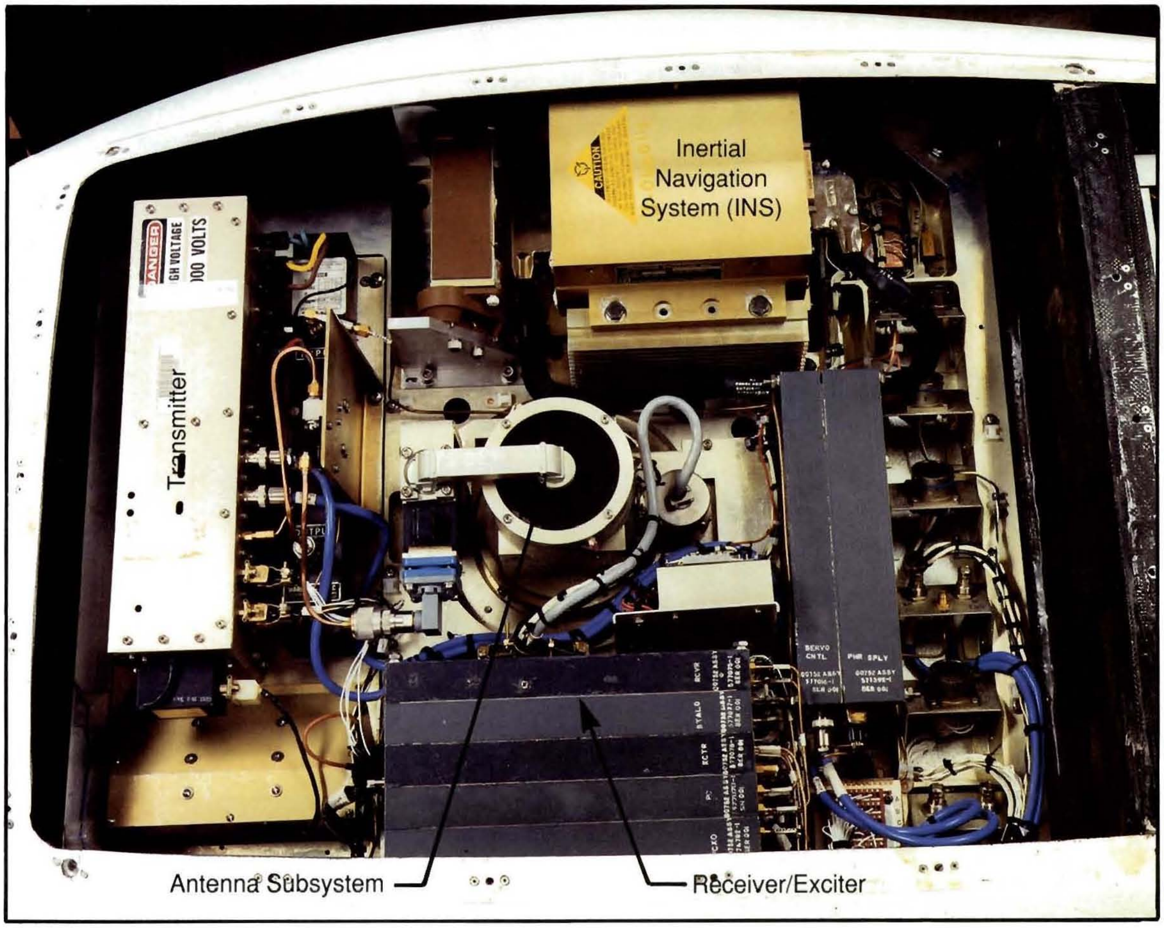

Fig. 20—Radar mounted in forward payload bay of UAV fuselage.

only power to the payload, and physical support to the UAV fuselage and radar.

All of the radar system components intended for UAV free flight—the Ku-band radar transceiver, the signal processor, and the various supporting components such as the UAV INS, narrowband data link, and antenna system—were assembled in an operational configuration inside the captive UAV fuselage (Figs. 20 and 21). For monitoring and recording data from the radar system, the manned aircraft carries the following instrumentation and display equipment: a two-way wideband data link, a DELCO Carousel IV INS, an autopilot, and a beacon-interrogation system that provides the manned aircraft with a complete and independent system for measuring its location and attitude. As mentioned earlier, a GPS receiver will eventually be used to update the UAV INS after a sufficient number of GPS satellites have been launched.

Radar moving-target reports as well as the

Fig. 21—Parabolic dish antenna mounted in UAV fuselage.

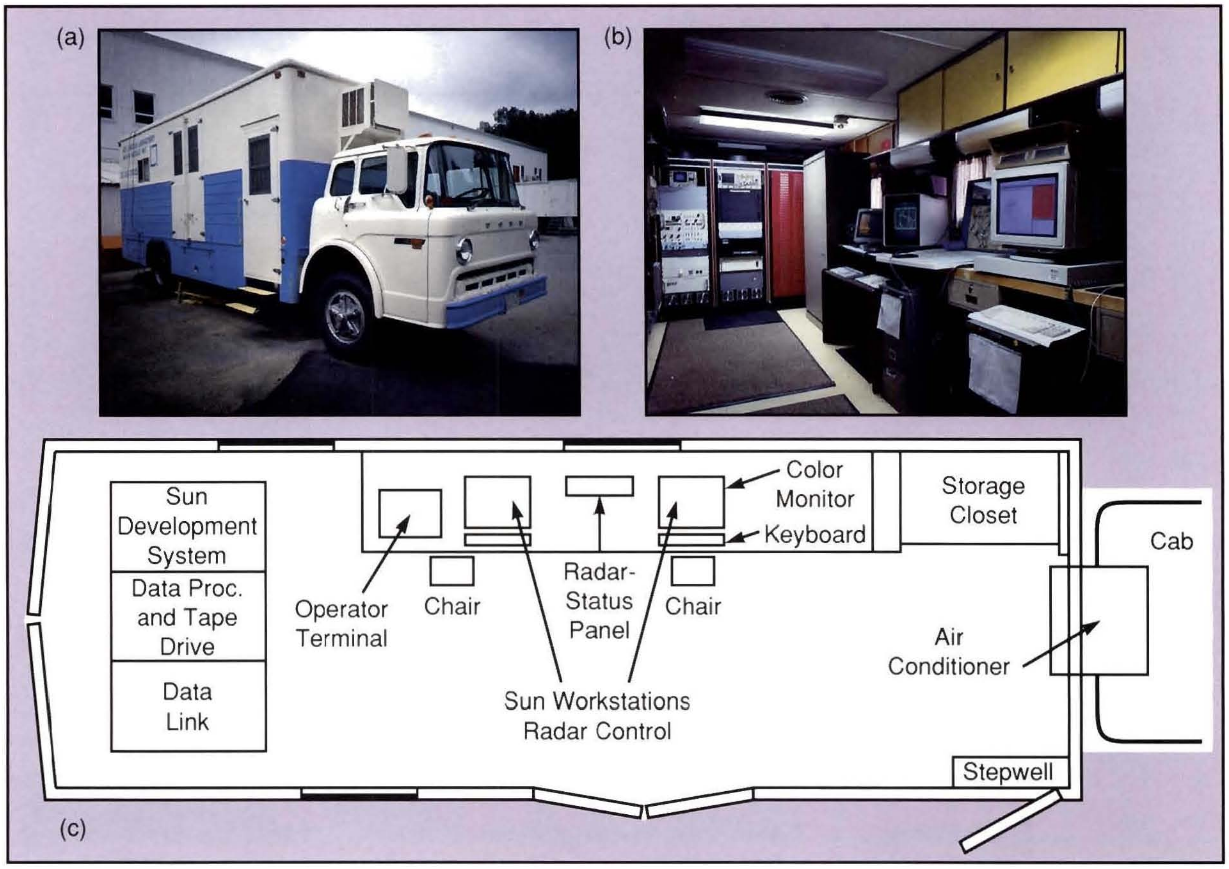

Fig. 22—Experimental ground terminal van for UAV radar: (a) exterior, (b) interior, and (c) plan view of interior layout.

current radar-mode information and INS data are sent down the wideband data link to the ground terminal van while radar-mode control commands are sent uplink. Thus an operator in the van can control the radar and view the target detections on a display in real time. The 10-W CW FM data link, which is a portable C-band autotracking unit, was manufactured by AACOM Co. and adapted for our purposes without concern for the link's military specification requirements or electronic-countermeasure susceptibility. The data link's range and azimuth coverage are 30 km and 360°, respectively.

The ground terminal van (Fig. 22) contains a data-link interface, communications equipment, a 68020 general-purpose processor, a digital recording system, a display monitor, and the operator control terminal. The general functions of the ground terminal equipment are to allow ground control of the radar modes, perform track-while-scan target tracking, receive/display target detections and track information, supply UAV data to a general communications network, and provide playback capability based on recorded data.

Test Results

We conducted tests to assess the system's accuracy in determining the positions of detected moving targets, as well as to assess the overall system performance. Although the tests were done in captive-flight operation with a DELCO INS and a beacon system for the determination of platform location and attitude, we believe the results are indicative of the UAV radar's performance in free flight.

Accuracy of UAV Radar System

For the major sources of error associated with a single detection of a moving target, we evaluated a primary error budget. Target-location errors are directly related to the location error of the UAV itself, an error that is estimated to be less than 50 m. In addition, when the INS heading errors (4 mrad), beamsplitting errors (6 mrad), and other miscellaneous errors were combined in a root of the sum of the squares (RSS) manner, the total angle error was found to be 8.5 mrad. This angle error dominates the range error and produces a cross-range error of 85 m at a range of 10 km. Combining the 50-m and 85-m errors in an RSS manner results in a position error estimate that is less than 100 m.

Using an electronic moving-target simulator (MTS), we tested the system's position accuracy for moving-target detections. An MTS is a device that intercepts a radar signal, amplifies it, and shifts its carrier frequency—just as a real moving target would—and then sends the signal back to the radar. If the MTS is located at an accurately surveyed position on the ground, we can use the measurements to calculate the range and angle biases in the UAV radar system. The measured biases can then be used to correct measurements of the moving-target detections.

Figure 23 is a plot of "moving" targets that the UAV system detected as the radar was flown in a 10-km circle around a stationary MTS. On a UTM grid, the figure plots the system's 354 estimates of the MTS's location. Because the observations were taken over a full circle, the errors in locating the MTS are indicative of the cross-range errors of the system. The 50-m resolution waveform was used, and the resulting one-sigma range error was 16 m. The cross-range error corresponded favorably to the calculated estimate from the primary error budget. However, our results were obtained with an ideal target; i.e., the MTS had a 30-dB SNR and the MTS returns were nonfluctuating. Furthermore, we used a radar scanning rate of 10°/s. The use of a faster scanning rate (such as

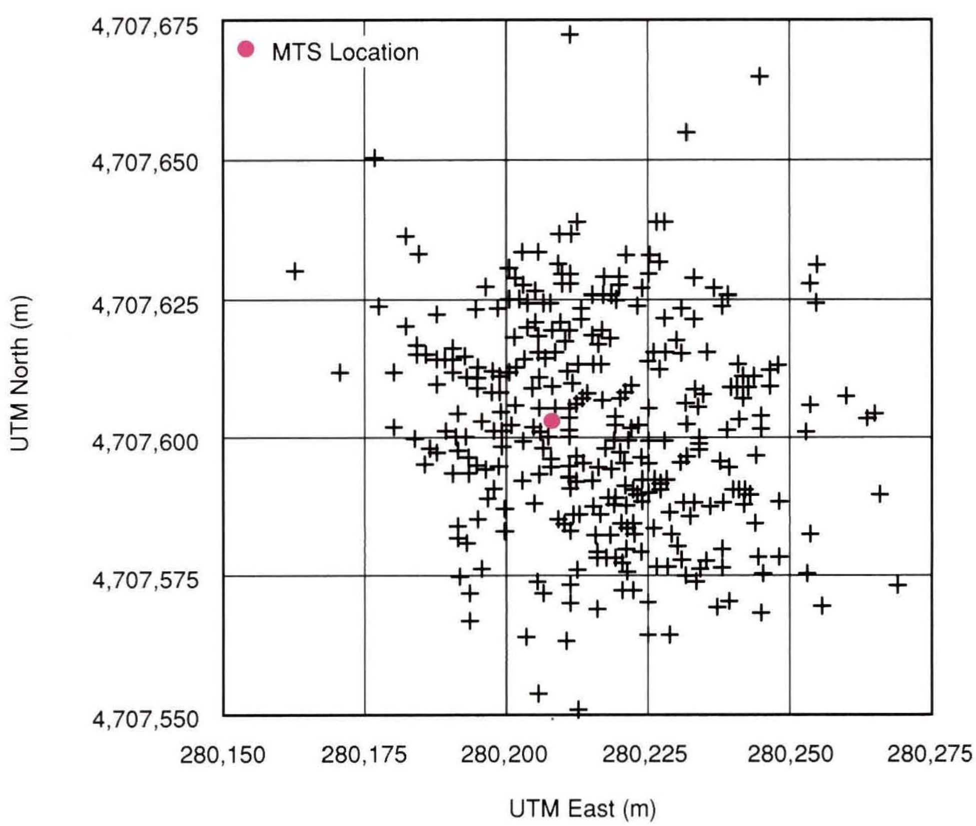

Fig. 23—Plot of "moving" targets that the UAV system detected as the radar was flown in a 10-km circle around a stationary moving-target simulator (MTS). The figure contains the UAV radar system's 354 estimates of the MTS's location. The one-sigma range error is 16 m.

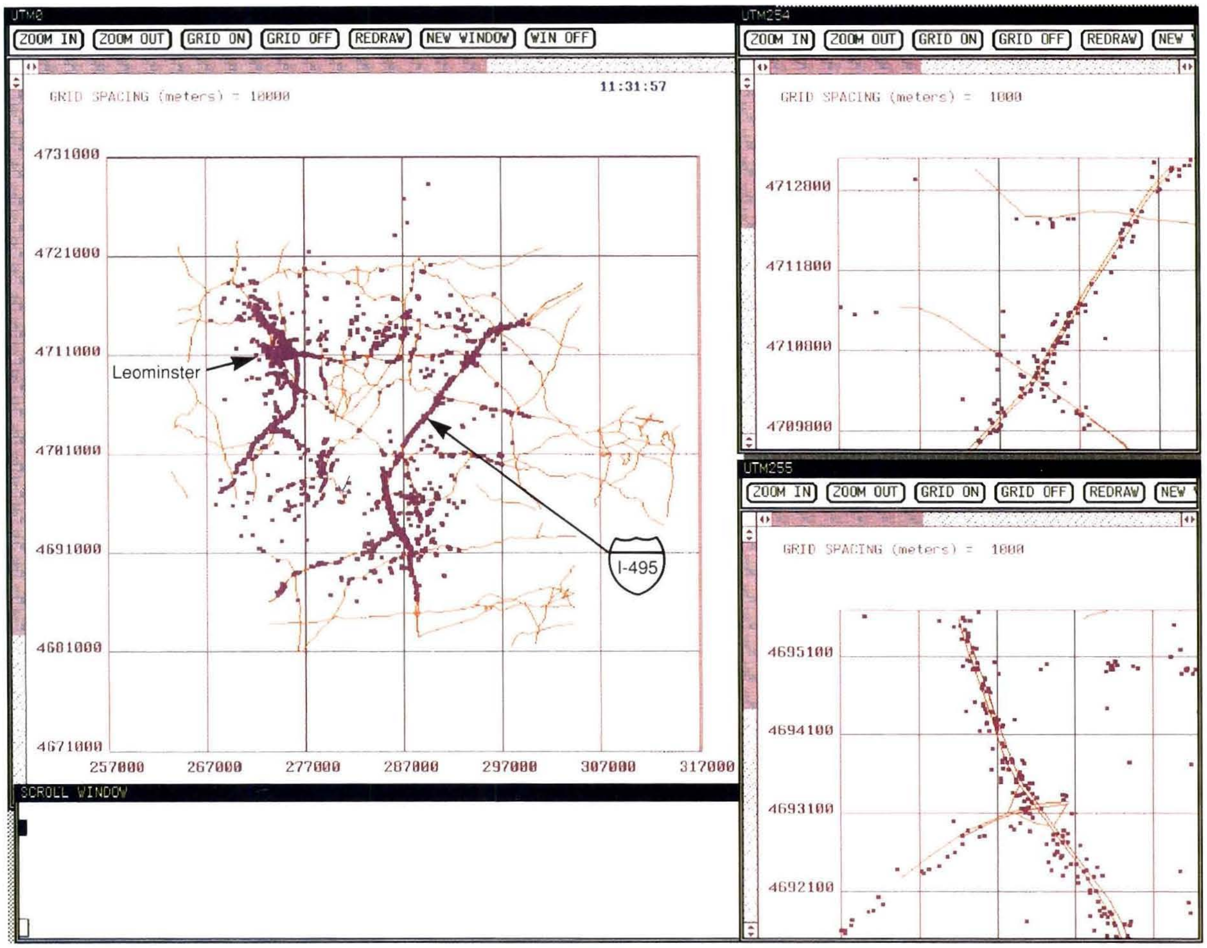

Fig. 24—Van operator's display showing 3.5 min of moving-target reports during a test in which the UAV radar system was flown west of Boston above the town of Leominster and Interstate 495, a major highway with three lanes in each direction. The operator has selected three map windows. In the left window the operator is viewing the overall area. Some of the major roads in the area have been drawn as line segments, and a UTM grid is used for reference. The small black squares indicate the locations of moving-target reports from the UAV radar. On the right part of the display, the operator has chosen a higher resolution to monitor two road intersections. Note that the moving-target detections correlate well with the road locations.

20°/s) or measurements on smaller vehicles (such as automobiles) would result in larger location errors. Also, large tactical targets such as tanks and trucks can cause the radar returns to fluctuate.

Nonetheless, further captive-flight tests on military vehicles indicate that the cross-range error should be within the estimated error from the primary error budget. (The tests are described in greater detail in the following section.) We estimate that the error will be comparable after the GPS receiver is incorporated into the system. As stated earlier, we are currently emulating the position-update accuracy of a GPS-based system by using multilateration with ground beacon ranges to determine the platform location in real time. Further improvement can be obtained by the correlation of target measurements from scan to scan.

Test Results on Moving Targets

In captive-flight tests, the UAV radar system has detected vehicles traveling on the highways west of Boston in the vicinity of Interstate 495. Figure 24 is a picture of the ground van's real-time operator display from 3.5 min of moving-target reports. The radar is in the wide-area surveillance mode and the operator has selected three map windows on the display, which is manufactured by Sun Microsystems. In the left window the operator is viewing the overall area. Some of the major roads in the area have been drawn as line segments and a UTM grid is used for reference. The small black squares indicate the locations of moving-target reports from the UAV radar. On the right part of the display, the operator has chosen a higher resolution to monitor two road intersections. During the tests, a large number of moving targets were detected over an area of approximately 900 km^2, and the detections correlated well with the roads, as shown on the display. Note that an operator can easily discern the varying density of the traffic. The main road in the center of the map is I-495—a large highway with three lanes in each direction. Other smaller tree-lined roads nearby are also clearly visible.

During the tests, the plane flew at an altitude of 4500 ft and the radar antenna scanned a 360° azimuth sector at a rate of 20°/s. The radar was transmitting a 50-m-resolution waveform, and data from a range swath between 5 km and 15 km were processed. The PRF used corresponds to an unambiguous velocity interval of about ±29 m/s (±64 mph).

The operator in the van can also choose to display moving-target tracks that are generated by a tracker (Fig. 25). The tracker correlates

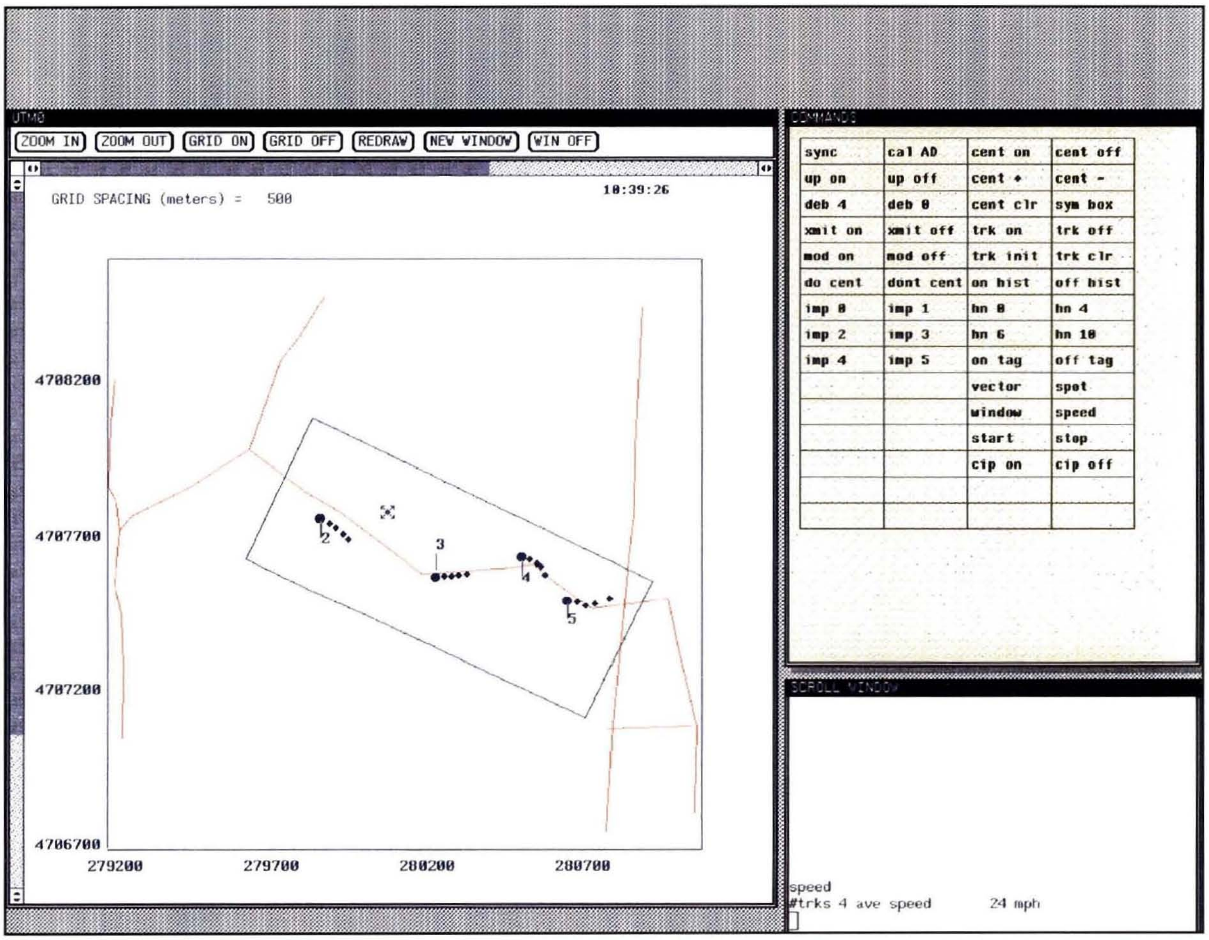

Fig. 25—Real-time display of four truck-size vehicles in track. The large dots represent the most recent locations of each vehicle and the smaller diamonds depict the history of previous location estimates. The cross symbol indicates the center of the current sector scan. The target numbers are used for reference by the operator to fetch more data on a particular track or to select target information that needs to be transmitted to another user. The processing algorithm automatically counts the number of vehicles in the operator-drawn box and displays the count (four vehicles) and their average speed (24 mph) in the lower right corner of the screen.

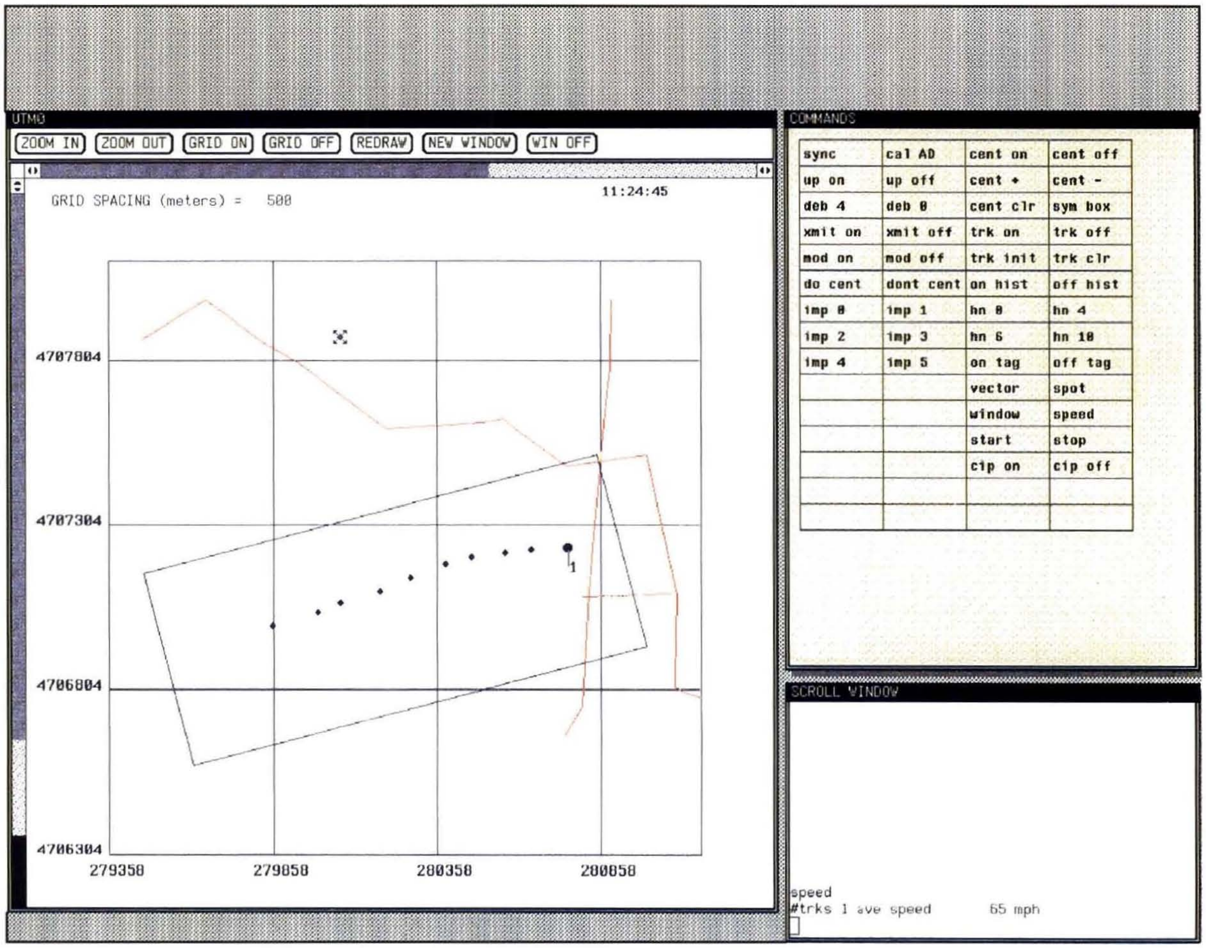

Fig. 26—Real-time display of a low-flying helicopter in track. The large dot represents the most recent estimate of the vehicle's location and the smaller diamonds depict the history of previous location estimates. The cross symbol indicates the center of the current sector scan. The operator has chosen to display nine previous estimates and the lower right corner of the screen indicates that one target traveling at 65 mph has been detected within the operator-drawn box.

moving-target reports from scan to scan to generate estimates of moving-target positions and velocities. For effective track association, vehicle measurements are needed every 5 s. The tracker uses the measured Doppler-based velocities and positions to initiate tracks and to associate measurements from one scan to another.

In Fig. 25, the operator has drawn a box around a truck convoy on a road west of Boston. The processing algorithm automatically counts the number of vehicles in the box and displays the count (four vehicles) and their average speed (24 mph) in the lower right corner of the screen. The large dots represent the most recent estimated locations of each vehicle. The smaller diamonds depict the history of previous estimates of the targets' locations. The target numbers can be used by the operator to fetch more data on a particular track or to select target information that needs to be transmitted to another user.

Figure 26 shows part of the track of a low-flying helicopter that flew into the test area. As in Fig. 25, the large dot represents the most recent estimate of the vehicle's location. The operator has chosen to display nine previous estimates to obtain the flight path of the helicopter, and the screen indicates that there is one target traveling at 65 mph within the operator-drawn box.

Currently, the tracker is configured to maintain files on 100 tracks. A much larger number of targets could be tracked if the processing power in the ground van is substantially increased.

The UAV radar system's 15-m waveform provides good resolution in range, but the 2.3° two-way azimuth beamwidth results in a 400-m cross-range resolution at a 10-km range. The large cross-range resolution limits the system's ability to separate individual vehicles in the azimuth direction.

Future Improvements and Applications

Although system weight was a major concern in designing the prototype UAV radar, our primary emphasis was on proving the feasibility of the system. A second prototype design could easily reduce the radar weight by 15 to 20 lb, which would result in a maximum weight of 90 to 95 lb for the radar system alone. In addition, elements of the support equipment such as the frame could be lightened.

Enhancements could also be made to increase the sensitivity of the radar and thereby increase its detection range. Two modifications that would contribute to such an increase are (1) a new low-noise amplifier in the front end that would decrease the system noise, and (2) a new antenna to provide more gain as well as elevation information for estimating target-aircraft altitude. The above hardware modifications coupled with additional signal processing could increase the system's range to 25 km.

The speed of the signal/data processor is currently limited by the speed of the custom VLSI NMOS AG and AP chips. To replace the chips, application-specific integrated circuits (ASIC) were designed with Seattle Silicon's ASIC compiler. The new AG chips, which have been fabricated in 1.5-μm CMOS, will support an increase in processor speed from 108 to 360 MOPS. The new AP chip is being fabricated in 1.25-μm CMOS and is expected to support the same increase in speed. Because the new chips are plug compatible with the existing ones, the current processors can be upgraded with simple one-for-one chip replacements.

Use of the ASIC compiler will ease future upgrades because once a chip is designed with the compiler the chip can be fabricated in a newer, higher-speed technology by a relatively simple recompilation in the new rule set. That is, the chip would not have to be redesigned. Seattle Silicon guarantees the delivery of packaged functioning chips that will correctly execute the simulation test vectors used to validate the chip design.

Increased processing capability is important to support new radar applications such as synthetic-aperture radar for stationary-target detection, adaptive jammer nulling, and air defense. UAV radars are not limited to ground surveillance; in fact, they could provide accurate surveillance of low-flying aircraft that cannot be detected by ground radars because of foliage or terrain masking. Or UAV radars could be used for the detection and tracking of ships at sea. Although the prototype system was specifically designed to detect moving targets on the ground, the system is programmable and can hence be reprogrammed to handle other types of applications. For example, to detect and track low-altitude, fixed-wing aircraft, the UAV radar could be reprogrammed to scan a limited azimuth sector more rapidly.

Summary

Current technology supports a UAV radar payload that detects moving ground vehicles and helicopters out to a range of 15 km. The payload can supply the battlefield commander with a real-time display of battlefield activity in all weather conditions, day or night. Information provided would include accurate vehicle location and velocity data, and the payload has limited target-classification capability.

Acknowledgments

The success of the UAV-radar program at Lincoln Laboratory is the result of the combined efforts and contributions of many dedicated people. The authors thank their group colleagues Ben Bader, Paula Caban, Cary Conrad, Bob Catalan, Elsa Chen, Dave Craska, John Duncan, Bob Giovannucci, Ed Hall, Don Malpass, Gary Provencher, Greg Rocco, Tom Sefranek, Keith Sisterson, Mike Spitalere, Sue Yao, and Alan Yasutovich. The valuable support of Warren Bebeau, Robin Fedorchuk, Michelle Hinkley, and Michele Kalenoski in the Laboratory's Battlefield Surveillance Group office is also appreciated. In addition, the authors acknowledge the significant contributions of Mike Judd and Al Benoit in the Laboratory's Engineering Division and George Knittel for the radome design.

The work described in this article was sponsored by the Army's LABCOM, Harry Diamond Laboratories, and the Defense Advanced Research Projects Agency (DARPA). The authors thank Jeff Sichina, John David, and Richard Slife of the Army's Harry Diamond Laboratories; and John Entzminger and Dominick Giglio of DARPA/TTO for their valuable advice and continuing support.

References

1. V.L. Lynn, "Terrain and Foliage Masking for Long-Range Surveillance: A Sample of Measurements in Central Germany," *Project Report TST-35*, Lincoln Laboratory (15 June 1979), DDC AD-B040205-L.
2. W.L. Post, "Line of Sight Considerations in the Fulda Gap Area of the Federal Republic of Germany," *Technical Report DELCS-TR-82-2*, U.S. Army ERADCOM Combat Surveillance & Target Acquisition Laboratory, Fort Monmouth, NJ (Sept. 1982).
3. M.I. Mirkin, C.E. Schwartz, and S. Spoerri, "Automated Tracking with Netted Ground Surveillance Radars," *Record of IEEE 1980 Intl. Radar Conf., Arlington, VA, 28–30 Apr. 1980*, p. 371.
4. C.E. Schwartz, "Netted Radar Program Final Report, Volume III: Airborne Ground Surveillance Radar," Lincoln Laboratory (30 Sept. 1981), DTIC #AD-B061852-L.
5. E.R Hooten and K. Munson, *Jane's Battlefield Surveillance Systems 1989–90* (Jane's Information Group, Alexandria, VA, 1989).
6. F.E. Hall and A.G. Rocco, Jr., "A Compact Programmable Array Processor," *Lincoln Laboratory J.* **2**, 41 (1989).

CARROLL EDWARD SCHWARTZ received a B.S. degree in physics from Columbia University. Since 1965 he has worked on the design of real-time radar systems, ranging from large Ballistic Missile Defense measurement radars to smaller tactical airborne and ground surveillance radars. His field of specialty includes real-time software, automatic target detection and tracking, and signal processing. After joining the technical staff of Lincoln Laboratory in 1972, Ed spent five years working on algorithms for the automatic real-time detection, tracking, and discrimination of ballistic targets. For three of those years, he worked on Kwajalein, Marshall Islands, where he led a group that tested the algorithms against missiles launched from Vandenburg Air Force Base. Ed is currently the Assistant Group Leader of the Laboratory's Battlefield Surveillance Group, which is responsible for building the UAV radar and its high-speed processor.

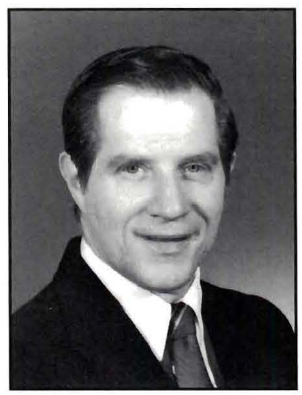

THOMAS G. BRYANT is a staff member in the Battlefield Surveillance Group at Lincoln Laboratory. During his 21 years at the Laboratory, which included three years on Kwajalein in the Marshall Islands, he has helped to develop various radar systems, including a millimeter-wave radar for a missile-seeker application. He is currently the project engineer for the unmanned air vehicle (UAV) radar system development program. His research interests include radar systems analysis, radar systems for airborne moving- and fixed-target detections, and associated signal processing. Tom received a B.S.E.E. degree and an M.S.E.E. degree from the University of Maine. He is a member of the IEEE, Eta Kappa Nu, Tau Beta Pi, Phi Kappa Phi, and Sigma Xi.

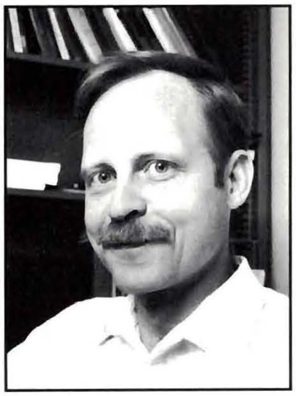

JAMES H. COSGROVE is an associate staff member in the Battlefield Surveillance Group at Lincoln Laboratory. Before joining the Laboratory 15 years ago, Jim worked for the U.S. Army. He received a B.S. degree in physics from the University of Massachusetts.

GERALD B. MORSE is Group Leader of Lincoln Laboratory's Battlefield Surveillance Group. His research interests include radars and signal processing. Before joining the Laboratory 25 years ago, Jerry worked for Varian Associates. He received a B.S. degree in physics from Northeastern University and an M.S. degree in physics from the Rensselaer Polytechnic Institute.

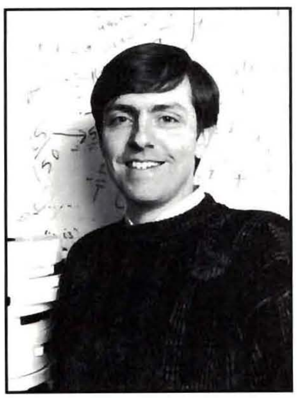

JAMES K. NOONAN received a B.A. degree in mathematics from Merrimack College and an M.S. degree in mathematics from Northeastern University. He worked for the National Security Agency before joining Lincoln Laboratory 10 years ago. Currently a staff member of the Laboratory's Battle Surveillance Group, he conducts research in radar signal processing algorithms and real-time systems. He is a member of Phi Kappa Phi.